Ocean Systems Engineering, *Vol. 12, No. 3 (2022) 285-300*
https://doi.org/10.12989/ose.2022.12.3.285

SPH simulation of solitary wave interaction with coastal structures

Guozhen Cai[1], Min Luo[*1], Zhaoheng Wei[1] and Abbas Khayyer[2]

[1]*Ocean College, Zhejiang University, Zhoushan, China*
[2]*Department of Civil and Earth Resources Engineering, Kyoto University, Kyoto, Japan*

(Received August 2, 2022, Revised September 9, 2021, Accepted September 12, 2022)

Abstract. This paper adopts the Smoothed Particle Hydrodynamics (SPH) open-source code SPHinXsys to study the solitary wave interaction with coastal structures. The convergence properties of the model in terms of particle size and smoothing length are tested based on the example of solitary wave propagation in a flat-bottom wave flume. After that, the solitary wave interactions with a suspended submerged flat plate and deck with girders are studied. The wave profile and velocity field near the surface of the structures, as well as the wave forces exerted onto the structures are analyzed.

Keywords: coastal structure; solitary wave; SPH; submerged deck; wave-structure interaction

1. Introduction

Coastal structures such as breakwaters, coastal docks and coastal bridges play significant roles in protecting the coastal areas and underpinning the economy. In practice, it is crucially important to design these structures properly such that they can survive under the actions of disastrous waves. Tsunami is a kind of disastrous wave that possesses tremendous energy and can cause serious damage to coastal structures. In this context, this paper studies the interaction between coastal structures and solitary wave, which resembles tsunami in terms of the key properties.

For investigating wave-structure interaction problems, the Computational Fluid Dynamics (CFD) modelling has been becoming prevailing due to the rapid development of computer hardware and numerical algorithms. Numerical models can be generally categorized into the mesh-based and meshless methods according to the way of discretizing the computational domain. A family of meshless methods is the so-called Lagrangian particle method that possesses advantageous features in dealing with large deformation and moving interface. According to how fluid pressure is solved, the particle methods are grouped into weakly-compressible methods and projection-based methods (imposing incompressibility strictly). The most famous and commonly-used method in the former group is the Smoothed Particle Hydrodynamics (SPH) (Amicarelli *et al.* 2020, Domínguez *et al.* 2021, Hérault *et al.* 2010, Kazemi and Luo 2022, Lyu *et al.* 2022, Monaghan 1994, Zhang *et al.* 2021a), while the latter group includes the Moving Particle Semi-implicit (MPS) method (Khayyer and Gotoh 2011, Koshizuka *et al.* 1998), Incompressible Smoothed Particle Hydrodynamics (ISPH)

*Corresponding author, Professor, E-mail: min.luo@zju.edu.cn

http://www.techno-press.org/?journal=ose&subpage=7 ISSN: 2093-6702 (Print), 2093-677X (Online)

(Chow *et al.* 2022, Shao and Lo 2003, Shimizu *et al.* 2022), Meshless Local Petrov Galerkin (MLPG) (Ma 2005) and Consistent Particle Method (CPM) (Luo *et al.* 2016, Luo *et al.* 2019, Luo *et al.* 2022). Comprehensive reviews of the latest developments and applications of particle methods are referred to Gotoh *et al*. (2021), Khayyer *et al*. (2022), Luo *et al*. (2021) and Sriram and Ma (2021).

In terms of modelling tsunami or solitary wave interaction with coastal structures, Wei *et al*. (2015) used SPH code GPUSPH to study the tsunami impact on piers with different shapes and different tsunami impact directions, as well as analyze the flow field around pier, river bed shear stress and the resulted hydrodynamic load. Followed, Wei and Dalrymple (2016) studied the tsunami impacts on the superstructures of a coastal bridge and examined the effectiveness of adding up-wave service road and offshore breakwater in reducing tsunami actions. Tripepi *et al.* (2020) applied the δ-SPH model to study the induced force of solitary waves on submerged horizontal cylinders and calibrated the hydrodynamic coefficients of resistance, inertia and lift force components in empirical formulas. Thereafter, the authors also studied the interaction of solitary waves with square barriers, focusing on the semi-analytical estimation of horizontal loads. Pringgana *et al*. (2021) used SPH open-source code DualSPHysics to investigate the effect of orientation and arrangement of land structures on tsunami impacts. In the category of the projection-based methods, Luo *et al*. (2019) studied the solitary wave interaction with seawalls using CPM. The influence of seawall cross section geometry was analyzed, as well as a simple and practical method was proposed to estimate tsunami intensity. Wang *et al*. (2020) used the MPS method to simulate the motion characteristics of the solitary wave on the inclined seawall and analyzed the wave overtopping characteristics.

The weakly-compressible SPH code SPHinXsys (Zhang *et al.* 2021a) has been undergoing rapid developments and has been used for wave-structure interaction problems, but simulations about solitary waves have been rarely reported. With the background illustrated above, this study adopts SPHinXsys to study the solitary wave interaction with fixed submerged coastal structures. The key hydrodynamic parameters including wave elevation and wave force will be elaborated in comparison with published experimental and numerical results. The physics behind the wave-structure interaction process is discussed, as well as the accuracy of SPHinXsys is verified. In what follows, Section 2 introduces the basic theory of SPHinXsys; Section 3 presents model validation as well as results and discussion; Section 4 gives concluding remarks on the numerical study.

2. Mathematical formulations

2.1 Governing equations

The governing equations are the continuity equation and Navier-Stokes (NS) equations in the Lagrangian form as follows

$$\begin{cases} \dfrac{D\rho}{Dt} = -\rho\nabla\cdot\mathbf{v} \\ \dfrac{D\mathbf{v}}{Dt} = -\dfrac{1}{\rho}\nabla p + \dfrac{\eta}{\rho}\nabla^2\mathbf{v} + \mathbf{g} \end{cases} \tag{1}$$

where ρ is the density of a fluid, $\mathbf{v}$ the particle velocity vector, p the fluid pressure, η the dynamic viscosity, $\mathbf{g}$ the gravity acceleration, and t is the time. The fluid domain is discretized by non-connecting particles. Each particle carries a fixed mass and moves under the combined action of the gravity, pressure gradient and viscous force as described in Eq. (1).

The present work adopts the weakly-compressible SPH method, more specifically, the SPHinXsys open-source code. The fluid pressure is solved through an equation of state (Zhang *et al.* 2021a)

$$p = c_0^2(\rho - \rho_0) \tag{2}$$

where ρ_0 is the reference density, c_0 is the artificial speed of sound adopted to be 10 times of the projected maximum particle velocity during the simulation.

2.2 Numerical formulations of SPHinXsys

The governing equations are discretized in the particle interpolation framework as follows (Zhang *et al*. 2021b)

$$\begin{cases} \dfrac{D\rho_i}{Dt} = 2\rho_i \displaystyle\sum_j \frac{m_j}{\rho_j}(\mathbf{v}_i - \overline{\mathbf{v}}_{ij}) \cdot \nabla_i W_{ij} \\ \dfrac{D\mathbf{v}_i}{Dt} = -2\displaystyle\sum_j m_j \frac{\overline{p}_{ij}}{\rho_i \rho_j} \nabla_i W_{ij} + 2\sum_j m_j \frac{\eta}{\rho_i \rho_j} \frac{\mathbf{v}_{ij}}{r_{ij}} \frac{\partial W_{ij}}{\partial r_{ij}} + \mathbf{g}_i \end{cases} \tag{3}$$

where $\overline{\mathbf{v}}_{ij} = (\mathbf{v}_i + \mathbf{v}_j)/2$, $\overline{p}_{ij} = (p_i + p_j)/2$; m_j is the mass of particle j which is fixed during the simulation; W is the kernel function used in particle interpolation. A fifth-order Wendland kernel function (Wendland 1995) is adopted in the present study

$$W = \alpha_{\mathrm{d}} \begin{cases} \left(1 - \dfrac{1}{2}q\right)^4 (1 + 2q), & 0 \le q < 2 \\ 0, & q \ge 2 \end{cases} \tag{4}$$

where α_d is a constant equal to $7/(4\pi h^2)$ for two-dimensional simulations, and $q = |\mathbf{r}_i - \mathbf{r}_j|/h = r_{ij}/h$ with h being the smoothing length.

A key feature of the SPHinXsys code lies in the adoption of the Riemann solver (Zhang *et al*. 2017) to mitigate numerical noises (e.g., the spurious pressure fluctuation). In the Riemann solver, an imaginary interface is constructed between two particles, and the states at the left and right sides of the interface are as follows (more details are referred to Zhang *et al.* (2021b))

$$\begin{cases} (\rho_L, U_L, P_L, c_L) = (\rho_i - \mathbf{v}_i \cdot \mathbf{e}_{ij}, p_i, c_i) \\ (\rho_R, U_R, P_R, c_R) = (\rho_j - \mathbf{v}_j \cdot \mathbf{e}_{ij}, p_j, c_j) \end{cases} \tag{5}$$

where L and R indicate left and right, respectively.

A low-dissipation Riemann solver is adopted as follows

$$\begin{aligned} \mathbf{v}^* &= \frac{1}{2}(\mathbf{v}_i + \mathbf{v}_j) - (U^* - \frac{1}{2}(U_L + U_R)) \cdot \mathbf{e}_{ij} \\ U^* &= \frac{(\rho_L c_L U_L + \rho_R c_R U_R + P_L - P_R)}{\rho_L c_L + \rho_R c_R} \\ p^* &= \frac{(\rho_L c_L P_R + \rho_R c_R P_L + \rho_L c_L \rho_R c_R \beta (U_L - U_R))}{\rho_L c_L + \rho_R c_R} \end{aligned} \tag{6}$$

where $\beta = \min(3\max(U_L\text{-}U_R, 0)/c, 1)$ denotes the low dissipation limiter and $c = (\rho_L c_L + \rho_R c_R)/(\rho_L + \rho_R)$. The variables of p^* and $\mathbf{v}^*$ are then used to replace the terms $\bar{p}_{ij}$ and $\bar{\mathbf{v}}_{ij}$ in Eq. (3). This leads to the particle-interpolated continuity and momentum equations.

For the time marching, the time step size is determined based on the CFL condition as follows

$$\Delta t = CFL \frac{h}{c + v_{\max}} \tag{7}$$

where the coefficient *CFL* is adopted to be 0.6 and h is the smoothing length (a parametric study with respect to it will be conducted).

In SPHinXsys, the wall boundaries of the submerged obstacle and the computational domain are modelled by dummy particles. The interaction between fluid particles and wall particles is modelled by solving a one-sided Riemann problem along the wall normal direction. In the one-sided Riemann problem, the left state is defined as $(\rho_L, U_L, P_L) = (\rho_f, -\mathbf{n}_w \cdot \mathbf{v}_f, P_f)$, where the subscripts f and w represent fluid and wall particles, as well as $\mathbf{n_w}$ is the local wall normal direction.

By applying the non-slip wall condition, the right state (i.e., wall particles) velocity U_R can be calculated by $U_R = -U_L + 2u_w$, where u_w is the wall velocity. The Neumann boundary condition is applied for pressure. Specifically, the pressure values on wall particles are calculated by $P_R = P_L + \rho_f \mathbf{g} \cdot \mathbf{r}_{fw}$, where $\mathbf{r}_{fw} = \mathbf{r}_w - \mathbf{r}_f$ with $\boldsymbol{r}_w$ and $\mathbf{r}_f$ being the positions of a wall particle and its relating fluid particle. Substituting the solved pressure into the equation of state, the right-state density can then be calculated (Zhang *et al.* 2017).

3. Numerical examples

3.1 Solitary wave generation

3.1.1 Solitary wave generation theory

The surface elevation of the Boussinesq-type solitary wave reads (Goring 1978)

$$\eta = H \operatorname{sech}^2 \left[k(x - ct) \right] \tag{8}$$

where H is the wave height, c the wave speed and t the time. Letting the initial water depth be h, the wave celerity can be approximated as

$$c = \sqrt{g(h + H)} \tag{9}$$

and the parameter k can be evaluated as

$$k = \sqrt{\frac{3H}{4h^3}} \tag{10}$$

The particle method, due to its Lagrangian nature, can model the moving wave maker with ease. Therefore, the present study adopts the moving wave maker approach among the others (Luo *et al.* 2021). For this, a simplified time series function of the wavemaker movement is adopted, as follows (Anbarsooz *et al.* 2013, Farhadi *et al*. 2016, Wang *et al.* 2020)

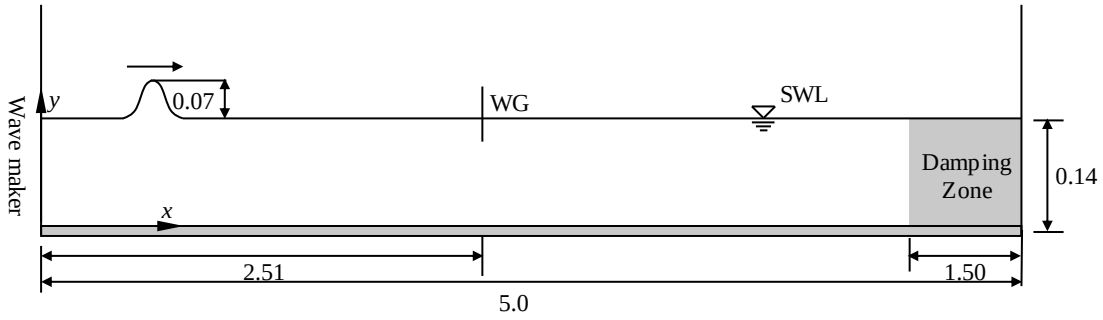

Fig. 1 Computational domain of solitary wave generation and propagation (unit: m)

$$X(t) = S \cdot \tanh\left(7.6\left(\frac{t}{\tau} - \frac{1}{2}\right)\right) \tag{11}$$

where S is the stroke of the wave maker and τ is the duration of the wave maker movement, computed respectively as

$$S = \sqrt{\frac{16H}{3h}}h \tag{12}$$

$$\tau = \frac{2}{kc}\left(3.80 + \frac{H}{h}\right) \tag{13}$$

3.1.2 Validation of numerical model

The computational domain of solitary wave generation is sketched in Fig. 1. The solitary wave of height H = 0.07 m is propagating over a flat bottom domain of initial water depth h = 0.14 m. The effective fluid domain length is 6.5 m. At the downstream side of the domain, a sponge layer of length 1.5 m is placed to dissipate wave energy and hence minimize the wave reflection. The fluid particles in the sponge layer are subjected to excessive viscous force and their velocities are governed by $\mathbf{v} = \mathbf{v}_0(1.0 - \Delta t\alpha(\frac{\mathbf{r} - \mathbf{r}_0}{\mathbf{r}_1 - \mathbf{r}_0}))$, where $\mathbf{v}_0$ is the initial velocity of a fluid particle just entering the damping zone, Δt the time step, $\mathbf{r}_0$ and $\mathbf{r}_1$ the starting and ending locations of the damping zone, respectively, and $\mathbf{v}$ the velocity at the location $\mathbf{r}$. The coefficient α controls the damping intensity and is adopted to be 5.0 (Zhang *et al.* 2021b) in the present study.

The smoothing length and particle size are two important numerical parameters that affect the simulation accuracy and efficiency of the SPH method. Therefore, convergence studies with respect to the two parameters are conducted in comparison with the analytical solution. Regarding the former, four smoothing lengths, i.e. d_s = 1.3l_0, 1.5l_0, 1.7l_0 and 1.9l_0 are tested with the converged particle spacing, i.e., l_0 = 0.003 m (will be presented later). The wave elevations at x = 2.51 m (WG) under the four d_s values are presented in Fig. 2. The occurrence time of the wave crest predicted by the simulations of different d_s are very close, but the crest heights show discrepancies among different cases. The wave crest values and the computational time of the four cases are presented in Table 1. As can be seen, the relative errors of the predicted wave crests in the four d_s cases are -10%,

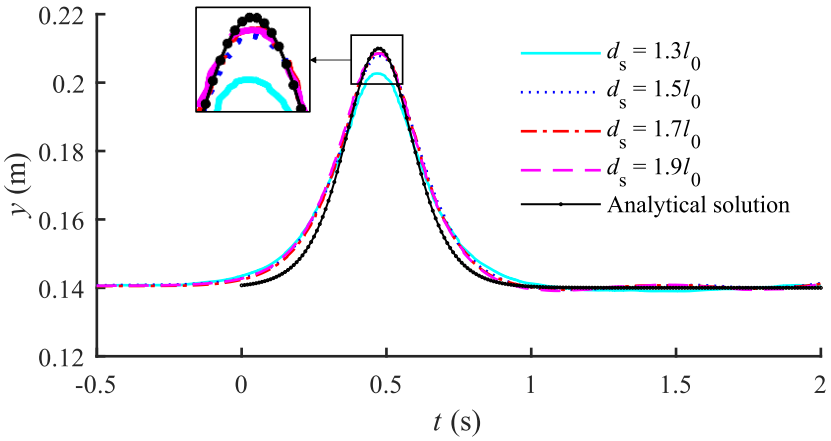

Fig. 2 Wave elevation at x = 2.51 m by using different smoothing lengths, d_s, with l_0 = 0.003 m

Table 1 Relative errors of computed wave height and computational efficiency by using different smoothing lengths, d_s, with the particle size of 0.003 m

Smoothing length (m)	1.3 l_0	1.5 l_0	1.7 l_0	1.9 l_0
Predicted wave height (m)	0.063	0.068	0.069	0.068
Relative error (%)	-10.00%	-2.86%	-1.43%	-2.86%
Computational time (s)	130	133	136	140

Table 2 Relative errors of computed wave height and computational efficiency by using different particle sizes, l_0, with the smoothing length of 1.7l_0

Particle size (m)	l_0 = 0.01	l_0 = 0.005	l_0 = 0.003	l_0 = 0.0025
Predicted wave height (m)	0.068	0.069	0.068	0.068
Relative error (%)	-2.86%	-1.43%	-2.86%	-2.86%
Computational time (s)	16	124	557	954

-2.86%, -1.43%, -2.86%, respectively. The computational time is 130 s, 133 s, 136 s and 140 s per physical second, respectively. On the tradeoff accuracy and efficiency, a smoothing length of d_s = 1.7l_0 is adopted in the present study.

Based on the smoothing length of d_s = 1.7l_0, the particle size convergence of the model is studied by testing four particle sizes, i.e., l_0 = 0.01 m, 0.005 m, 0.003 m and 0.0025 m. The wave elevations predicted by the four particle sizes are presented in Fig. 3, as well as the relative errors and computational efficiency are presented in Table 2. Among the four cases, the result by l_0 = 0.01 m shows the largest relative error (i.e., -2.86%) and the up-crossing side of the wave crest is not smooth. With l_0 = 0.005 m, an unphysical wave crest shape at the up-crossing side is also evident, although the predicted wave height is close to the analytical value. For the other two particle sizes, i.e., l_0 = 0.003 m and 0.0025 m, both results are very close and in satisfactory agreement with the analytical crest shape and the analytical wave height (relative errors being -2.86%). These show a good particle size convergence of the model. Note that the use of a fine particle size leads to a significant increase

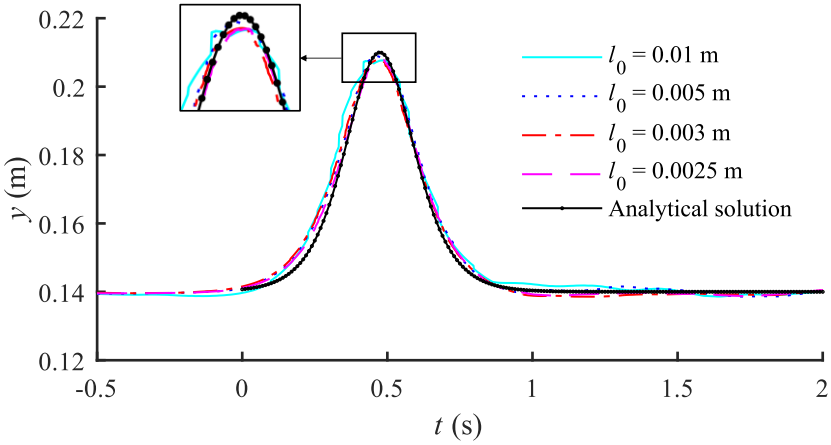

Fig. 3 Wave elevation at x = 2.51 m by using different particle sizes with $d_s = 1.7l_0$

of simulation time. Compromising accuracy and efficiency, the particle size of l_0 = 0.003 m is adopted in the present study (this also ensures that the structural dimensions are close to the integer multiplies of the particle size).

3.2 Solitary wave interaction with a submerged flat plate

The case of solitary wave interaction with a submerged flat plate is studied (Seiffert *et al.* 2014), in which the mesh sizes were Δx = 0.0025 m and Δz = 0.001 m, being smaller than the particle size used in the present simulation. As sketched in Fig. 4, the effective length of the computational domain is L = 7.84 m and a piston-type wave maker is placed on the left side of the domain. A fixed flat plate of width 0.305 m and thickness of 0.0127 m (0.013 m is adopted herein) is placed such that its leading edge (facing the incident wave) is 2.62 m from the initial location of the wave maker. Other parameters considered are: water depth h = 0.086 m, submergence ratio z/h = 0.2 (measured from the top of the plate to the still-water level) and solitary wave height $H = 0.287h$. In simulations, a fixed particle size is adopted to be l_0 = 0.003 m by considering the particle size convergence and letting each dimension of the structure be the integer multiplies of particle size. With this, the numerical domain contains a total of 102,591 particles and the computational time is about 74 minutes for simulating a physical time of 8 s. Studied include the wave elevations at three gauge locations (i.e., x = 2.01, 3.535, and 4.755 m denoted by WG1, WG2 and WG3, respectively), as well as the horizontal and vertical components of the wave force applied on the plate. Since the instant of t = 0 is not explained explicitly in the cited work, the timing of the present simulation results is adjusted such that the crest peaks at WG1 of the three sets of results occur at the same time.

The wave profiles and velocity fields at typical time instants of the wave-deck interaction process are presented in Figs. 5 and 6. As can be seen, the wave crest reaches the leading edge of the deck at t = 5.0 s. After that, the wave velocity underneath the deck is almost horizontal due to the confinement of the deck, while the wave above the deck shows the shoaling feature due to the reduction of the effective water depth. Especially, wave breaking happens when the wave crest passes the deck at around t = 5.4 s. The present SPH captures the whole process satisfactorily with regular particle and smooth pressure distributions.

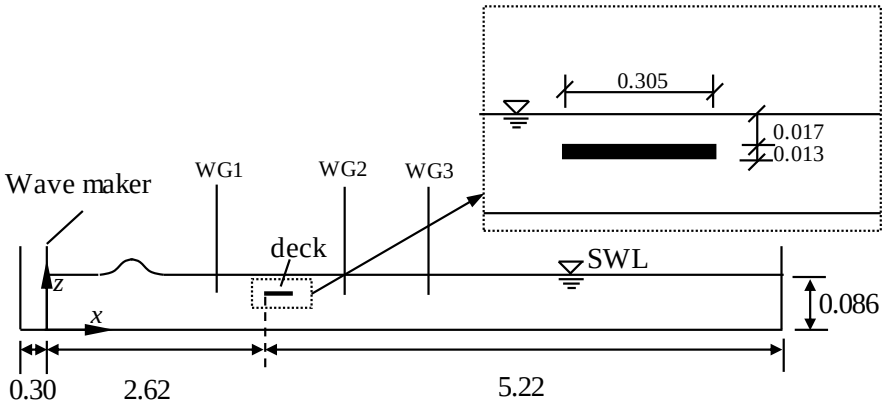

Fig. 4 Computational domain of solitary wave interaction with a flat plate (unit: m)

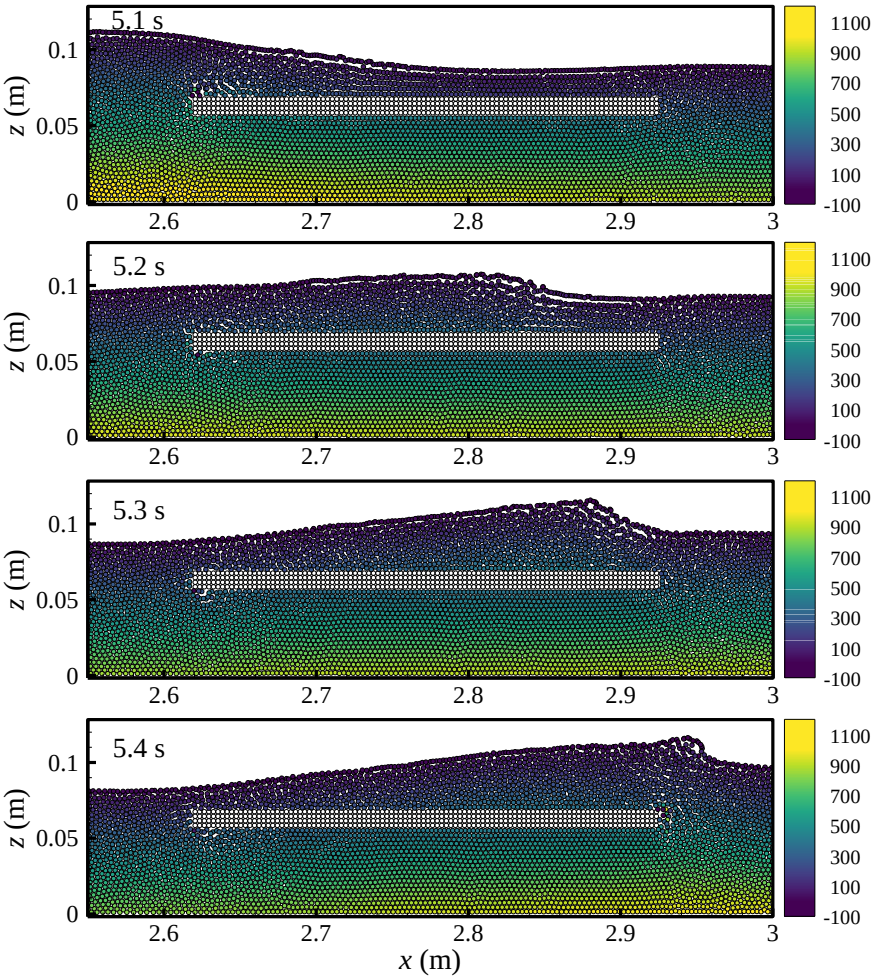

Fig. 5 Particle distributions with pressure contours near the plate at t = 5.0, 5.2, 5.3 and 5.4 s

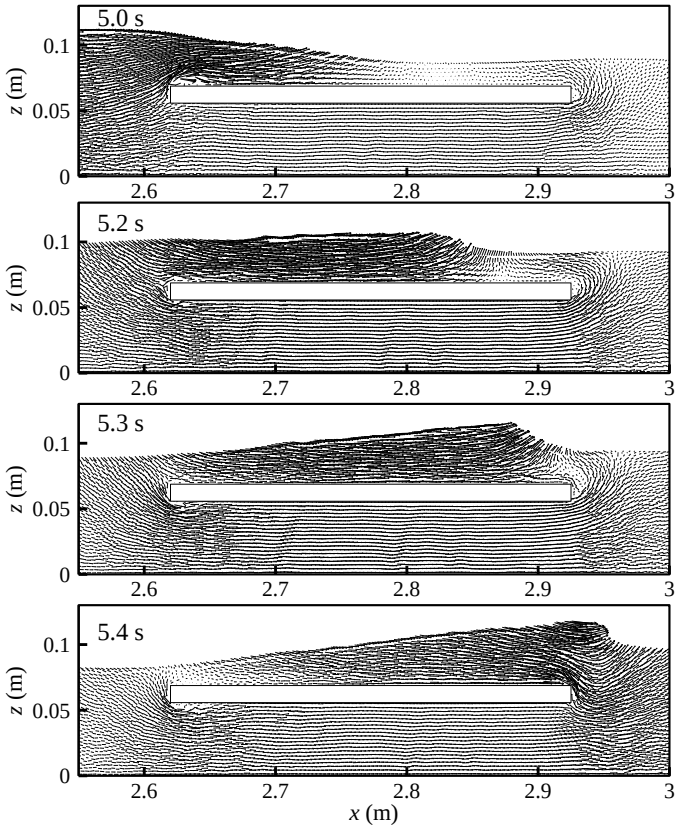

Fig. 6 Velocity fields near the plate at t = 5.0, 5.2, 5.3 and 5.4 s

The wave elevations and wave force components predicted by the present SPH model are compared with published results (Seiffert *et al.* 2014) in Figs. 7 and 8, respectively. From Fig. 7, the wave elevations measured in experiment manifested an evident decay from WG1 to WG2 and WG3, while the decays are much smaller in published OpenFOAM and the present SPH simulations. Specifically, the relative errors of the predicted peaks at WG2 and WG3 with respect to the experimental values are 36.5% and 38.8% in OpenFOAM, and 22.8% and 19.5% in SPH. Generally, the present SPH results are in a closer agreement with the experimental data.

Regarding the wave force presented in Fig. 8, the force components obtained by the present two-dimensional simulation are multiplied by the width of the physical water flume (i.e., 0.149 m) for comparison with the experimental data. For the vertical force F_z, the overall trend and magnitude predicted by the SPH model are in good agreement with the published experimental and OpenFOAM results. For the horizontal force F_x, the magnitude predicted by SPH is larger than that of the experimental result, while the OpenFOAM result was smaller. Besides, the SPH result does not show the negative force that was observed in experimental and OpenFOAM results. From the wave profile snapshot at t = 5.4 s, the particle distributions near the leading and trailing ends of the deck are not very regular. This leads to inaccuracy of pressure and hence force computation, which may be the reason for the above discrepancy.

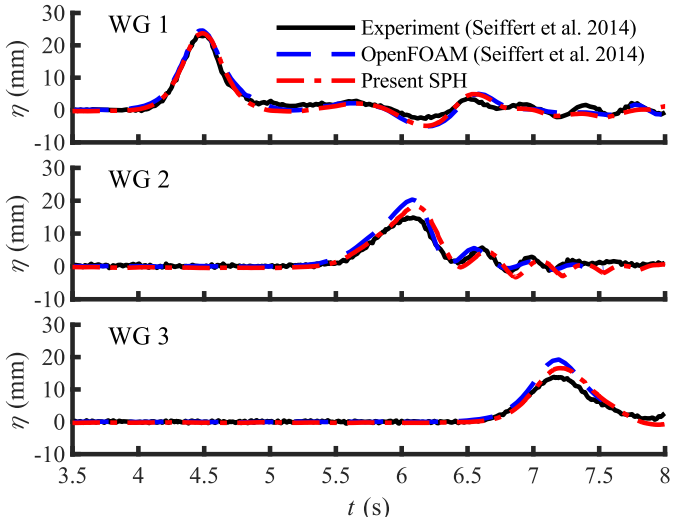

Fig. 7 Wave elevations at WG1, WG2 and WG3 in the case of solitary wave interaction with a flat plate

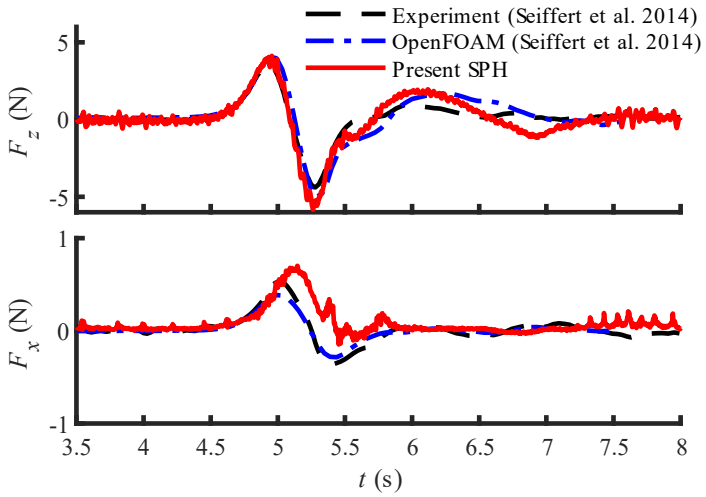

Fig. 8 Wave force components applied on the flat plate

3.3 Solitary wave interaction with deck with girders

This section studies the case of solitary wave interaction with a submerged deck with girders (Hayatdavoodi *et al*. 2014). The horizontal component of the deck is identical to the plate studied in Section 3.2, but with short vertical girders. The cross-sectional shape and dimensions of the deck are shown in Fig. 9. The computational setup including the domain size, water depth, wave parameter and structural location are the same as those in Section 3.2.

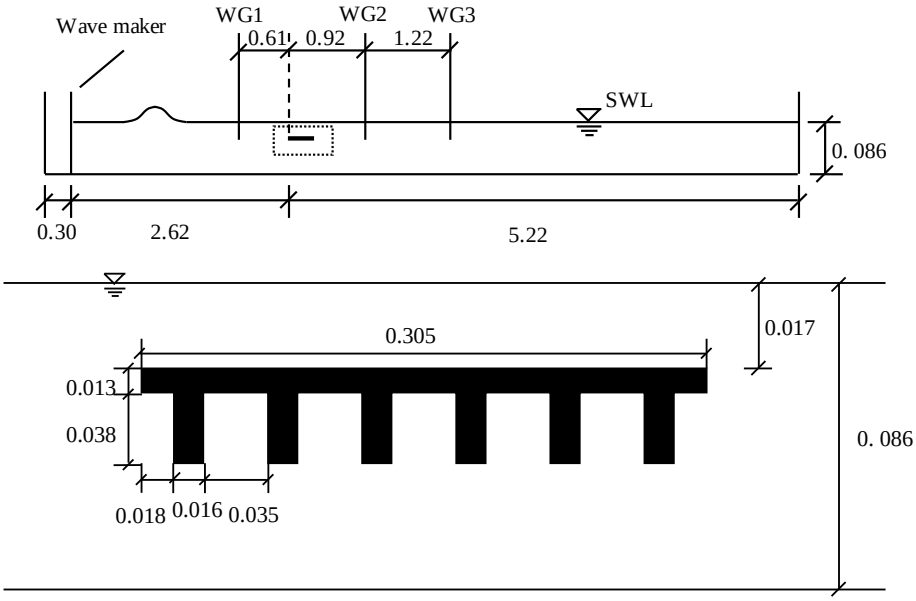

Fig. 9 Computational domain of solitary interaction with the deck with girders (unit: m)

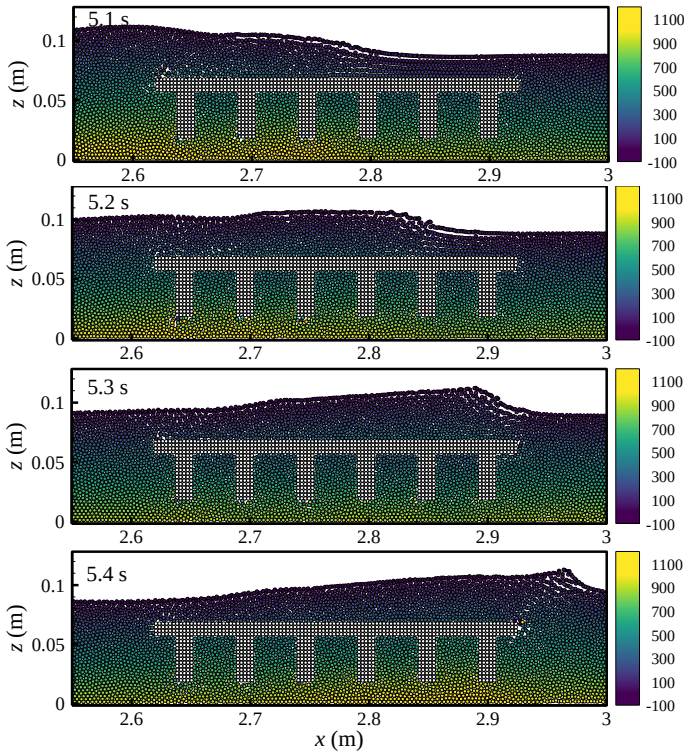

Fig. 10 Particle distributions and pressure contours at typical time instants in the case of solitary wave interaction with the deck with vertical girders

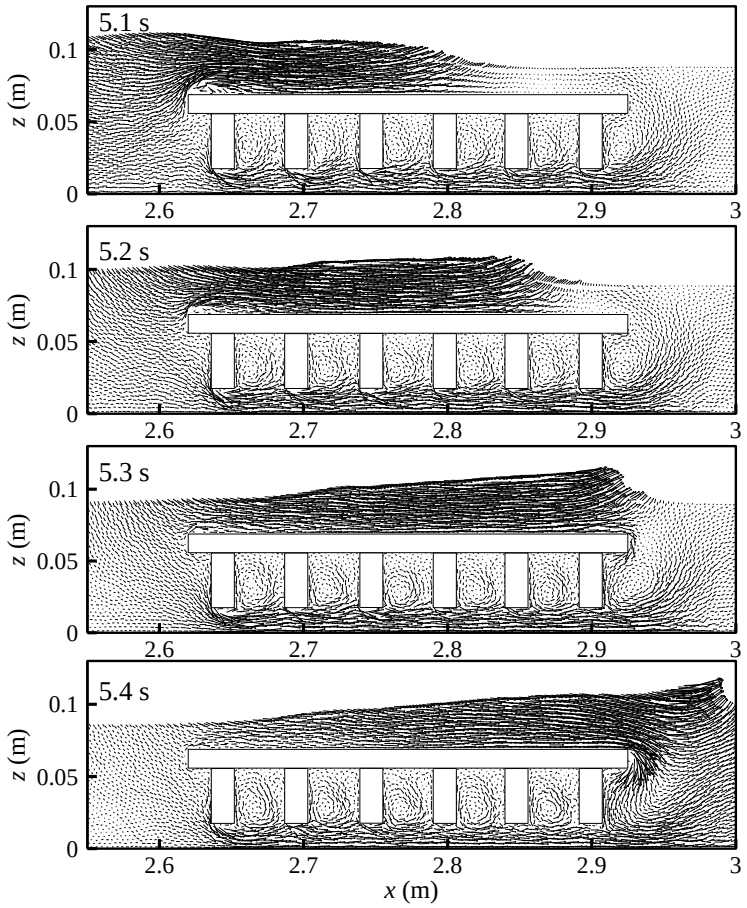

Fig. 11 Velocity fields at typical time instants in the case of solitary wave interaction with the deck with girders

The wave profiles and velocity fields at typical time instants are presented in Figs. 10 and 11. A distinct feature of wave underneath the deck as compared to the flat deck case is the vortexes induced by the wave-girder interaction, which dissipate wave energies. Above the deck, the shoaling process happens similarly to that in the case without girders. Again, the particle distribution and pressure distribution are generally smooth in the whole domain except for the regions near the leading- and trailing edges of the deck.

The wave elevations predicted by the present SPH model are compared with the experimental and OpenFOAM results (Hayatdavoodi *et al.* 2014) in Fig. 12. Similar to the case with a flat deck, the wave elevations decay from WG1 to WG3, but the numerical results decay much less than the experimental results. The relative errors of the simulated elevation peaks at WG2 and WG3 with respect to the experimental data are 40.82% and 76.03% for OpenFOAM, and 25.22% and 55.30% for SPH, being much smaller. It can also be seen that the wave elevation decay in the case with vertical girders is larger than that in the flat deck case due to the excessive energy dissipation induced by the girders.

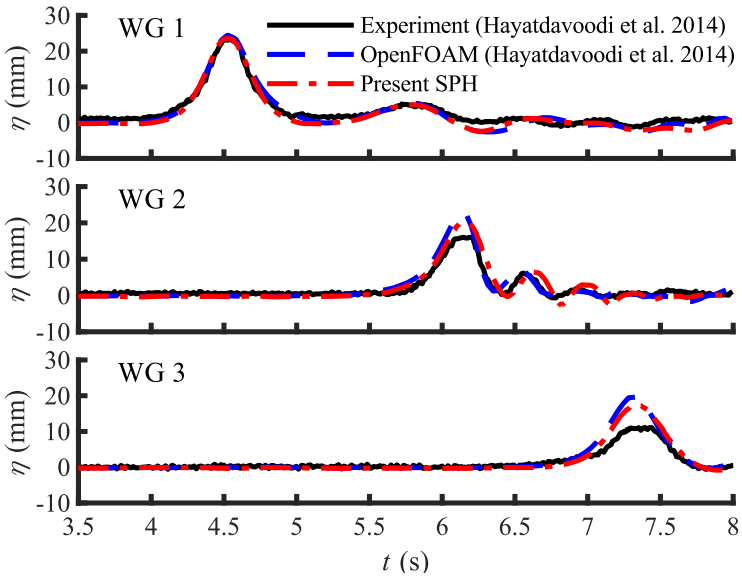

Fig. 12 Wave elevations in the case of solitary wave interaction with the deck with girders

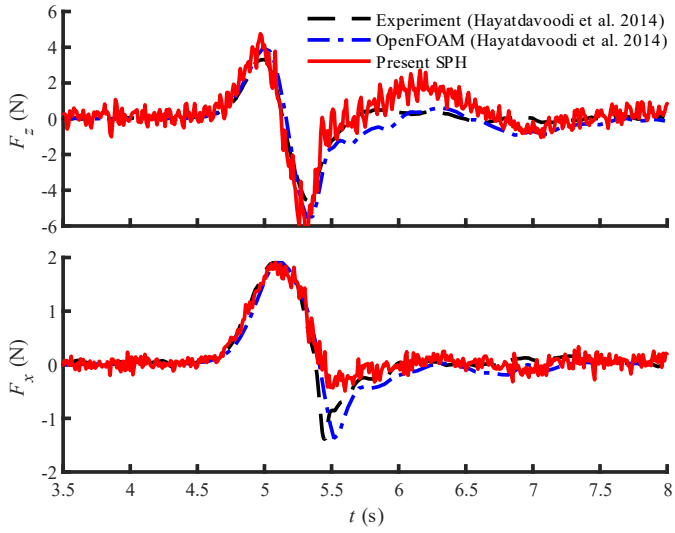

Fig. 13 Wave force components applied on the deck with girders

The wave forces applied on the deck are shown in Fig. 13. For the vertical force F_z, the overall trend and magnitude predicted by SPH are in good agreement with the published experimental and OpenFOAM results. For the horizontal force F_x, the positive peak predicted by SPH matches the published results well, but the predicted negative peak is much smaller. As compared to the flat deck

case, the magnitude of the horizontal force in the present case is larger because the vertical girders are subjected to considerable horizontal forces. Besides, larger fluctuations exist in the simulated force of the present case, which is partially because the vortexes induced by girders cause more violent dynamic pressures. Another reason for the fluctuation is attributed to numerical noises of the weakly compressible modelling, in which the fluid pressure is solved explicitly by using an equation of state that relates fluid pressure and density. Applying the kernel gradient correction scheme (Randles and Libersky 1996) (for improvement of kinematics) and an enhanced numerical resolution of continuity equation (for improvement of pressure, i.e., dynamics) can be helpful in mitigating the unphysical fluctuations in force prediction, which are our ongoing and future works.

4. Conclusions

This work adopts the SPH open-source code SPHinXsys for studying the interaction process of solitary wave passing through a submerged horizontal deck and a deck with short vertical girders.

The convergence of the model with respect to the particle smoothing length and particle size is firstly tested, based on which the smoothing length of $d_s = 1.7l_0$ and particle spacing of $l_0 = 0.003$ m are found to the convergent for the present solitary wave case.

By using the identified parameters, the cases of solitary wave interaction with flat plate deck and deck with girders are studied. In both cases, the simulated wave elevations show reductions as the wave passes through the structure. A similar trend was observed in the published OpenFOAM results although the documented experimental measurements showed a much larger reduction. Regarding the wave force, the vertical component predicted by SPH is in good agreement with the published ones, while the horizontal component by SPH shows a larger positive peak and no negative peak as compared to the documented experimental and OpenFOAM results. The discrepancies in the horizontal force are presumably related to the non-physical particle distribution at the leading- and trailing-edges of the deck, which could be partially resolved by using the numerical schemes like particle shifting.

Acknowledgements

The authors would like to express their sincere gratitude to the anonymous reviewers for the insightful and constructive comments that definitely helped in improving the paper. The authors are also grateful to Dr. Chi Zhang (Technical University of Munich) and Ms. Yaru Ren (Sichuan University) for their insightful comments. This research was supported by the start-up funding provided by Zhejiang University to the corresponding author.

References

Amicarelli, A., Manenti, S., Albano, R., Agate, G., Paggi, M., Longoni, L., Mirauda, D., Ziane, L., Viccione, G., Todeschini, S., Sole, A., Baldini, L.M., Brambilla, D., Papini, M., Khellaf, M.C., Tagliafierro, B., Sarno, L. and Pirovano, G. (2020), "SPHERA v.9.0.0: A Computational Fluid Dynamics research code, based on the Smoothed Particle Hydrodynamics mesh-less method", *Comput. Phys. Commun.*, **250**, 107157. https://doi.org/10.1016/j.cpc.2020.107157.

Anbarsooz, M., Passandideh-Fard, M. and Moghiman, M. (2013), "Fully nonlinear viscous wave generation in numerical wave tanks", *Ocean Eng*., **59**, 73-85. https://doi.org/10.1016/j.oceaneng.2012.11.011.

Chow, A.D., Stansby, P.K., Rogers, B.D., Lind, S.J. and Fang, Q. (2022), "Focused wave interaction with a partially-immersed rectangular box using 2-D incompressible SPH on a GPU comparing with experiment and linear theory", *Eur. J. Mech. - B/Fluid*., **95**, 252-275. https://doi.org/10.1016/j.euromechflu.2022.05.007.

Domínguez, J.M., Fourtakas, G., Altomare, C., Canelas, R.B., Tafuni, A., García-Feal, O., Martínez-Estévez, I., Mokos, A., Vacondio, R. and Crespo, A.J. (2021), "DualSPHysics: from fluid dynamics to multiphysics problems", *Comput. Particle Mech*., 1-29. https://doi.org/10.1007/s40571-021-00404-2.

Farhadi, A., Ershadi, H., Emdad, H. and Goshtasbi Rad, E. (2016), "Comparative study on the accuracy of solitary wave generations in an ISPH-based numerical wave flume", *Appl. Ocean Res*., **54**, 115-136. https://doi.org/10.1016/j.apor.2015.11.003.

Goring, D.G. (1978), Tsunamis--the propagation of long waves onto a shelf. California Institute of Technology.

Gotoh, H., Khayyer, A. and Shimizu, Y. (2021), "Entirely Lagrangian meshfree computational methods for hydroelastic fluid-structure interactions in ocean engineering—Reliability, adaptivity and generality", *Appl. Ocean Res*., **115**, 102822. https://doi.org/10.1016/j.apor.2021.102822.

Hayatdavoodi, M., Seiffert, B. and Ertekin, R.C. (2014), "Experiments and computations of solitary-wave forces on a coastal-bridge deck. Part II: Deck with girders", *Coast. Eng*., **88**, 210-228. https://doi.org/10.1016/j.coastaleng.2014.02.007.

Hérault, A., Bilotta, G. and Dalrymple, R.A. (2010), "SPH on GPU with CUDA", *J. Hydraul. Res*., **48**(1), 74-79.

Kazemi, E. and Luo, M. (2022), "A comparative study on the accuracy and conservation properties of the SPH method for fluid flow interaction with porous media", *Adv. Water Resour.*, **165**, 104220. https://doi.org/10.1016/j.advwatres.2022.104220.

Khayyer, A. and Gotoh, H. (2011), "Enhancement of stability and accuracy of the moving particle semi-implicit method", *J. Comput. Phys.*, **230**(8), 3093-3118. https://doi.org/10.1016/j.jcp.2011.01.009.

Khayyer, A., Gotoh, H. and Shimizu, Y. (2022), "On systematic development of FSI solvers in the context of particle methods", *J. Hydrodynam*., **34**, 395-407. https://doi.org/10.1007/s42241-022-0042-3.

Koshizuka, S., Nobe, A. and Oka, Y. (1998), "Numerical analysis of breaking waves using the moving particle semi-implicit method", *Int. J. Numer. Meth. Fl.*, **26**(7), 751-769. https://doi.org/10.1002/(SICI)1097-0363(19980415)26:7<751::AID-FLD671>3.0.CO;2-C.

Luo, M., Khayyer, A. and Lin, P. (2021), "Particle methods in ocean and coastal engineering", *Appl. Ocean Res*., **114**, 102734. https://doi.org/10.1016/j.apor.2021.102734.

Luo, M., Koh, C.G., Bai, W. and Gao, M. (2016), "A particle method for two-phase flows with compressible air pocket", *Int. J. Numer. Meth. Fl.*, **108**(7), 695-721. https://doi.org/10.1002/nme.5230.

Luo, M., Reeve, D.E., Shao, S., Karunarathna, H., Lin, P. and Cai, H. (2019), "Consistent Particle Method simulation of solitary wave impinging on and overtopping a seawall", *Eng. Anal. Bound. Elem*., **103**, 160-171. https://doi.org/10.1016/j.enganabound.2019.03.012.

Luo, M., Su, X., Lin, P., Khayyer, A. and Zhao, X. (2022), "Investigation of two-layer liquid sloshing by using the Consistent Particle Method", *Int. J. Offshore Polar Eng*., **32**(1), 7-15. https://doi.org/10.17736/ijope.2022.jc848.

Lyu, H.G., Sun, P.N., Miao, J.M. and Zhang, A.M. (2022), "3D multi-resolution SPH modeling of the water entry dynamics of free-fall lifeboats", *Ocean Eng*., **257**, 111648. https://doi.org/10.1016/j.oceaneng.2022.111648.

Ma, Q. (2005), "Meshless local Petrov–Galerkin method for two-dimensional nonlinear water wave problems", *J. Comput. Phys*., **205**(2), 611-625. https://doi.org/10.1016/j.jcp.2004.11.010.

Monaghan, J.J. (1994), "Simulating free surface flows with SPH", *J. Comput. Phys.*, **110**(2), 399-406. https://doi.org/10.1006/jcph.1994.1034.

Pringgana, G., Cunningham, L.S. and Rogers, B.D. (2021), "Influence of orientation and arrangement of structures on Tsunami impact forces: numerical investigation with smoothed particle hydrodynamics", *J. Waterw. Port Coast. Ocean Eng*., **147**(3), 04021006. https://doi.org/10.1061/(ASCE)WW.1943-5460.0000629.

Randles, P. and Libersky, L.D. (1996), "Smoothed particle hydrodynamics: some recent improvements and applications", *Comput. Method. Appl. M.*, **139**(1-4), 375-408. https://doi.org/10.1016/S0045-7825(96)01090-0.

Seiffert, B., Hayatdavoodi, M. and Ertekin, R.C. (2014), "Experiments and computations of solitary-wave forces on a coastal-bridge deck. Part I: Flat Plate", *Coast. Eng.*, **88**, 194-209. https://doi.org/10.1016/j.coastaleng.2014.01.005.

Shao, S. and Lo, E.Y.M. (2003), "Incompressible SPH method for simulating Newtonian and non-Newtonian flows with a free surface", *Adv. Water Resour.*, **26**(7), 787-800. https://doi.org/10.1016/S0309-1708(03)00030-7.

Shimizu, Y., Khayyer, A. and Gotoh, H. (2022), "An enhanced incompressible SPH method for simulation of fluid flow interactions with saturated/unsaturated porous media of variable porosity", *Ocean Syst. Eng.*, **12**(1), 63-86. https://doi.org/10.12989/ose.2022.12.1.063.

Sriram, V. and Ma, Q.W. (2021), "Review on the local weak form-based meshless method (MLPG): Developments and applications in ocean engineering", *Appl. Ocean Re*s., **116**, 102883. https://doi.org/10.1016/j.apor.2021.102883.

Tripepi, G., Aristodemo, F., Meringolo, D.D., Gurnari, L. and Filianoti, P. (2020), "Hydrodynamic forces induced by a solitary wave interacting with a submerged square barrier: Physical tests and δ-LES-SPH simulations", *Coast. Eng.*, **158**, 103690. https://doi.org/10.1016/j.coastaleng.2020.103690.

Wang, L., Jiang, Q. and Zhang, C. (2020), "Numerical simulation of solitary waves overtopping on a sloping sea dike using a particle method", *Wave Motion*, **95**, 102535. https://doi.org/10.1016/j.wavemoti.2020.102535.

Wei, Z. and Dalrymple, R.A. (2016), "Numerical study on mitigating tsunami force on bridges by an SPH model", *J. Ocean Eng. Mar. Energy*, **2**(3), 365-380. https://doi.org/10.1007/s40722-016-0054-6.

Wendland, H. (1995), "Piecewise polynomial, positive definite and compactly supported radial functions of minimal degree", *Adv. Comput. Math.*, **4**(1), 389-396. https://doi.org/10.1007/BF02123482.

Xu, G. and Cai, C.S. (2015), "Numerical simulations of lateral restraining stiffness effect on bridge deck–wave interaction under solitary waves", *Eng. Struct.*, **101**, 337-351. https://doi.org/10.1016/j.engstruct.2015.07.031.

Zhang, C., Hu, X.Y. and Adams, N.A. (2017), "A weakly compressible SPH method based on a low-dissipation Riemann solver", *J. Comput. Phys.*, **335**, 605-620. https://doi.org/10.1016/j.jcp.2017.01.027.

Zhang, C., Rezavand, M., Zhu, Y., Yu, Y., Wu, D., Zhang, W., Wang, J. and Hu, X. (2021a), "SPHinXsys: An open-source multi-physics and multi-resolution library based on smoothed particle hydrodynamics", *Comput. Phys. Commun.*, **267**, 108066. https://doi.org/10.1016/j.cpc.2021.108066.

Zhang, C., Wei, Y., Dias, F. and Hu, X. (2021b), "An efficient fully Lagrangian solver for modeling wave interaction with oscillating wave surge converter", *Ocean Eng.*, **236**, 109540. https://doi.org/10.1016/j.oceaneng.2021.109540.

MK